*Molecular Simulation*, Vol. 29 (10–11), October–November 2003, pp. 697–709

Taylor & Francis
Taylor & Francis Group

# Molecular Simulations of Knudsen Wall-slip: Effect of Wall Morphology

GAURAV ARYA, HSUEH-CHIA CHANG and EDWARD J. MAGINN*

*Department of Chemical Engineering, University of Notre Dame, Notre Dame, IN 46556, USA*

*(Received September 2002; In final form January 2003)*

**This work involves a molecular simulation study of the phenomena of wall slip occurring in rarefied gases flowing through micro- and nano-channels. A simulation strategy that mimics a scattering experiment is developed in order to compute the tangential momentum accommodation coefficient ($f$) which governs the degree of slip at the wall surface. Noninteracting gas molecules are bombarded at an atomic wall composed of rigid atoms with suitably distributed velocities and a tangential drift velocity that simulates flow. The accommodation coefficient is computed from the loss in the tangential momentum of these molecules. The accommodation coefficient is observed to be strongly dependent on the physical roughness of the wall, as characterized by the parameter $\sigma_{wg}/L$, and the attractiveness of the wall to the fluid, as characterized by the parameter $\epsilon_{wg}/k_BT$, where $\sigma_{wg}$ and $\epsilon_{wg}$ are the Lennard–Jones interaction parameters of the wall and gas atoms while $L$ is the lattice unit length. The accommodation coefficient is found to be independent of the tangential drift velocity at small drift velocities commensurate to those observed in micro devices. The accommodation coefficient is also found to be independent of the inertial mass of the gas molecules. The dependence of $f$ on the two main governing factors has been presented in convenient "phase diagrams" plots. We also show a means of separating gases based on the differences in the accommodation coefficients of the various components in the mixture. Using molecular dynamics simulations, we show that separation factors higher than 20 are achieved for gases flowing through nanometer wide channels in the Knudsen regime. We also present a simple analytical model to determine the lower bound on the separation factor of the two gases.**

*Keywords*: Molecular dynamics; Wall-slip phenomenon; Knudsen number; Rarefied gases; Tangential momentum accommodation coefficient; Kinetic separation of gases

## INTRODUCTION

It is well known that fluids flowing through channels can undergo slip at the wall-fluid interface, thereby violating the venerable no-slip boundary condition of continuum hydrodynamics. Wall slip commonly occurs for dilute gases flowing at moderate to large Knudsen numbers ($Kn > 10^{-3}$), where the Knudsen number is defined as the ratio of the mean free path to a characteristic length scale, in this case, the diameter of the channel. Wall slip is rare for dense gases and liquids [1,2], though there are a few exceptions. For example, certain polymers and long hydrocarbons have been shown to undergo wall-slip at surfaces [3–5]. Liquids also tend to undergo slip under very high shear rates [6–8], or in the presence of hydrophobic or repulsive walls [9].

The amount of slip occurring is generally characterized by the slip coefficient $\zeta$, which relates the slip velocity $u_s$ to the velocity gradient at the surface $dv/dy$ by the following equation [10,11]

$$u_s = \zeta \frac{dv}{dy} \tag{1}$$

The phenomenon of wall slip becomes increasingly important as the channel dimensions shrink below the micrometer length scale; at these small length scales, the total fluid flow rate becomes highly dependent on the amount of the slip at the surface. For instance, in the case of a gas undergoing Poiseuille flow through a straight pore of circular cross section, the molar flow rate $Q$ is

*Corresponding author. Tel.: +1-574-631-5687. Fax: +1-574-631-8366. E-mail: ed@nd.edu; URL: http://www.nd.edu/ ~ed

ISSN 0892-7022 print/ISSN 1029-0435 online © 2003 Taylor & Francis Ltd
DOI: 10.1080/0892702031000103257

given by [11]

$$Q = -\frac{\pi a^4 n}{8\eta}\left(1 + 4\frac{\zeta}{a}\right)\frac{\mathrm{d}P}{\mathrm{d}x} \tag{2}$$

where $a$ is the radius of the pore, $\eta$ is the shear viscosity, $n$ is the molecule number density, and $\mathrm{d}P/\mathrm{d}x$ is the pressure gradient along the pore. From Eq. (2), it can be seen that when the radius $a$ becomes small, the contribution of the slip coefficient term, as given by the ratio $\zeta/a$, becomes large. Examples of technologically relevant systems for which fluid wall slip may be important are microelectromechanical systems (MEMS) devices, adsorbents such as carbon molecular sieves, catalyst particles, computer disk drives [12] and carbon nanotubes [13].

Experimental observation of wall slip is extremely difficult, especially in those systems having pores on the nanometer length scale. As described in the next section, several groups have tried to determine slip in confined systems using a variety of techniques. These experimental methods typically rely on indirect methods for measuring slip, and arrive at slip lengths through application of classical models. It is not at all clear, however, if these classical models are applicable on the nanometer length scale. Moreover, there is no direct means for predicting how a given fluid or fluid mixture will behave when flowing in a particular confined media. It is to be expected that molecular level details such as the nature of the solid surface, the interaction energy of the fluid with the surface, and the architecture of the fluid molecules themselves will play a role on the degree of slip. The objective of the present study is to examine how these and other parameters control the amount of slip observed for a fluid flowing at high Knudsen number. In addition, the validity of the classical models of slip will be tested. The approach involves the use of molecular dynamics to simulate the relevant slip processes at the atomistic level.

## BACKGROUND

### Theory

The classic theory for determining the slip coefficient $\zeta$ is due to Maxwell [10,11]. Briefly, the theory assumes that for gas flow in a channel, some fraction $f$ of the molecules colliding with the wall are diffusely reflected. The symbol $f$ is referred to as the *tangential momentum accommodation coefficient*. Diffuse reflections can be envisioned as resulting from adsorption at the wall, where molecules thermalize and are later re-emitted with a velocity entirely independent of the velocity with which they hit the wall. The rest of the molecules (i.e. the fraction $1-f$) are assumed to undergo specular reflection. These molecules do not lose any of their tangential momentum upon collision. Maxwell showed that the slip coefficient $\zeta$ in Eq. (1) can be related to $f$ as follows. The flux of molecules hitting the walls, $J$, is given by

$$J = \frac{1}{4}n\bar{c} \tag{3}$$

where $\bar{c}$ is the mean speed of the molecules, assumed to follow kinetic theory

$$\bar{c} = \left(\frac{8k_\mathrm{B}T}{\pi m}\right)^{1/2} \tag{4}$$

where $m$ is molecular mass and $T$ is the temperature. It is further assumed that the tangential velocity of the impinging molecules, $v$, is much smaller than $\bar{c}$. The tangential momentum flux, $\tau$, communicated with the wall due to the diffusely reflected molecules is given by

$$\tau = \frac{1}{4}fn\bar{c}mv \tag{5}$$

Very close to the wall there exist two types of molecules. Half of the molecules are impinging on the wall with a velocity $v$, while the other half are being reflected either diffusely or specularly with average tangential velocity $(1-f)v$. The slip velocity at the wall is therefore, the average of the tangential velocity of the impinging and reflected molecules as given by

$$u_\mathrm{s} = \frac{v + (1-f)v}{2} = \left(\frac{2-f}{2}\right)v \tag{6}$$

By definition, the tangential momentum flux is also given by the Newton's law of viscosity

$$\tau = \eta\frac{\mathrm{d}v}{\mathrm{d}y} \tag{7}$$

Thus the slip coefficient, defined in Eq. (1), is related to the accommodation coefficient $f$ by the following relation

$$\zeta = \frac{2\eta}{nm\bar{c}}\left(\frac{2-f}{f}\right) \tag{8}$$

which is Maxwell's classical result. Note that the slip coefficient becomes unbounded when all the molecules hitting the wall are specularly reflected (i.e. when $f = 0$).

The expression in Eq. (8) clearly indicates the importance of the accommodation coefficient $f$ in determining the amount of wall slip at the solid surface. Differences can be exploited to perform a kinetic separation of gases. For example, the separation factor $S_\mathrm{AB}$ for the two gases flowing in

a pore is defined as the ratio of the fluxes of the two components

$$S_{AB} = \frac{J_A}{J_B} = \frac{\int_{-l_y}^{l_y} n_A(y) v_A(y)\, dy}{\int_{-l_y}^{l_y} n_B(y) v_B(y)\, dy} \tag{9}$$

where $2l_y$ is the width of the slit-pore occupied by fluid molecules. The density profiles for each component, $n_A$ and $n_B$ will typically vary across the width of the pore as depicted by their respective dependence on the $y$ coordinate in Eq. (9).

The flow velocity of the two gases may be described by a Poiseuille flow with a slip velocity as given by

$$v_i(y) = -\left(\frac{\nabla P}{2\eta_i}\right)[l_y^2 - y^2 + 2\zeta_i l_y] \tag{10}$$

where the subscript $i$ refers to gases A or B. In the Knudsen regime, the slip coefficient for species $i$ is assumed to obey Maxwell's theory of slip, as given by

$$\zeta_i = \frac{2\eta_i}{n_i m_i \bar{c}_i}\left(\frac{2 - f_i}{f_i}\right) \tag{11}$$

To demonstrate this kind of separation more effectively, let us assume that the density of the two gases is *uniform* across the width of the pore. Also, let us assume that the two densities are equal, i.e. $n_A(y) = n_B(y) = n$. In addition, let us assume that the shear viscosities and the molar masses of the two species are also equivalent, i.e $\eta_A = \eta_B = \eta$ and $m_A = m_B = m$. The two gases are, therefore, identical to each other and differ only in the way they interact with the pore wall, as described by the inequality in their accommodation coefficients or the slip coefficients. Consider the case where $f_A < f_B$ (or $\zeta_A < \zeta_B$). Integrating the velocity profiles in Eq. (10), by using the expressions in Eq. (9) then yields

$$S_{AB} = \frac{1 + 3\zeta_A/l_y}{1 + 3\zeta_B/l_y} \tag{12}$$

Substituting Eq. (11) into the above result yields the following expression for the separation factor

$$S_{AB} = \frac{1 + \frac{6\eta}{nm\bar{c}l_y}\left(\frac{2-f_A}{f_A}\right)}{1 + \frac{6\eta}{nm\bar{c}l_y}\left(\frac{2-f_B}{f_B}\right)} \tag{13}$$

Using the fact that the Knudsen number is defined as follows

$$Kn = \frac{1}{2\sqrt{2}\pi n l_y d_i^2} \tag{14}$$

where $d_i$ is the diameter of gas molecule $i$, Eqs. (4), (13) and (14) may be combined to yield

$$S_{AB} = \frac{1 + \Gamma_A Kn}{1 + \Gamma_B Kn} \tag{15}$$

Note that $\Gamma_A > \Gamma_B$ where the parameter $\Gamma_i$ for species $i$ is given by

$$\Gamma_i = 33.41 \frac{\eta d_i^2}{\sqrt{m_i k_B T}}\left(\frac{2 - f_i}{f_i}\right) \tag{16}$$

The factor 33.41 in the above equation arrives from the convolution of various factors in the equations used to derive it.

Equation (15) is important because it suggests that gases having the same nominal properties (density, viscosity, mass) but different accommodation coefficients may be kinetically separated in the Knudsen regime due to their differences in slip behavior. Note that this separation capability is lost at small Knudsen numbers where $S_{AB}$ tends to unity. A canonical example of kinetic gas separation is oxygen and nitrogen in carbon molecular sieves [14]. Separation factors (or selectivities) between 3 and 30 for oxygen over nitrogen have been reported in the literature. These selectivities have been noted to be rather high considering that the two species differ only slightly in their size. The above analysis suggests that the high selectivities achieved in the above case are possibly due to the difference in which the two species interact with the wall, or more precisely, their respective slip coefficients or accommodation coefficients with respect to the carbon pore walls.

## Experiments

The determination of accommodation coefficients for various gases and surfaces has been the subject of several experimental studies. Loyalka *et al.* [15–18] used a steel spinning rotor gauge to measure the accommodation coefficient for a number of gases in both the slip and continuum regimes. Arkilic *et al.* [19] determined accommodation coefficients for nitrogen, argon and carbon dioxide in silicon micromachined channels under a variety of Knudsen numbers. Rettner [12] used molecular beam scattering to determine the accommodation coefficient for various surfaces of relevance to the disk-drive air bearing. In all these cases, imperfect accommodation was observed, with $f$ ranging from 0.80 to 0.96. The experiments also indicated that the accommodation coefficient is highly dependent on the nature of the solid surface. For instance, the value of the accommodation coefficient depends on whether the surface is free of adsorbed molecules and microscopically smooth or is contaminated and possesses a high degree of roughness [20]. The value of the accommodation coefficient also depends on the type of gas molecule, its energetic interactions with the surface, its translational velocity and the temperature [5,20]. Exactly how the accommodation coefficient depends on the above properties of the surface

and gas molecules remains unclear from the experiments.

### Simulations

To gain greater fundamental insight into the behavior of fluids near surfaces, molecular simulations have been adopted by researchers to simulate wall slip [21–23] and to understand the effect of surface morphology on wall slip [24–28]. Several studies have shown that repulsive walls tend to promote slip while attractive walls tend to produce no-slip boundary conditions [24–27]. It has also been observed that wall density and stiffness both play a role in governing wall slip, as they impact the effective surface roughness [27]. The linear slip velocity dependence on the shear rate at low shear rates has also been validated in one of the simulation studies [28]. Though the above simulation studies have greatly increased our insight into the qualitative features involved in wall slip, our understanding of the slip mechanisms remains largely incomplete. It is still not possible to predict slip behavior in real systems, nor is our understanding of the behavior of confined mixtures complete. What we require are *quantitative* methods for predicting the magnitude of the accommodation coefficient, and how it depends on the properties of the surface and gas.

The present study is a first step toward this objective. A molecular simulation strategy analogous to a scattering experiment has been developed to compute the accommodation coefficient for gases flowing over a model solid surface in the high Knudsen regime. Key dimensionless parameters related to the properties of the gas molecules and the wall surface are identified, and their impact on the accommodation coefficient has been determined. Finally, since the flow rate of fluids in channels is closely related to the accommodation coefficient, it is shown how kinetic separation of gases in nanopores may be controlled by wall slip. This is done by performing molecular dynamics simulations of gas mixtures within pores under a pressure gradient.

## METHODOLOGY

### Simulation System

The accommodation coefficient $f$ can be computed directly from its definition as given by

$$f \equiv \frac{(v_{\text{imp}} - v_{\text{ref}})}{v_{\text{imp}}} \tag{17}$$

where $v_{\text{imp}}$ is the *average* tangential velocity with which the gas molecules are impinging on the surface, while $v_{\text{ref}}$ is the average tangential velocity with which the molecules are reflected from the surface.

A schematic showing the essence of the simulation methodology is shown in Fig. 1. Gas molecules are created in the plane $y = y_0$, at which point the potential interaction with the wall is zero. These molecules are assigned velocities in the three directions according to a predetermined input distribution for the desired temperature $T$. Details regarding the initial velocity distribution are discussed below. A velocity of magnitude $v_{\text{imp}}$ is then superimposed onto the existing velocities in one of lateral directions (the $x$-component in Fig. 1) to mimic fluid flow down the channel. The trajectories of the colliding gas molecules are followed using molecular dynamics in the microcanonical ensemble. Molecules interact with the wall via a Lennard–Jones (LJ) potential. The average velocity of the reflected gas molecules along the channel (i.e. the reflected "drift" velocity) is subsequently computed to yield $v_{\text{ref}}$. The tangential momentum accommodation coefficient $f$ is thereby computed using Eq. (17).

To model Knudsen flow of rarefied gases, gas molecules are not allowed to interact with each other. The trajectories followed by the various gas molecules are therefore, independent of each other. To obtain an accurate value of $v_{\text{ref}}$, a large number of collisions with the wall are required to adequately sample the spectrum of incident velocities and collision angles. The number of collisions that must

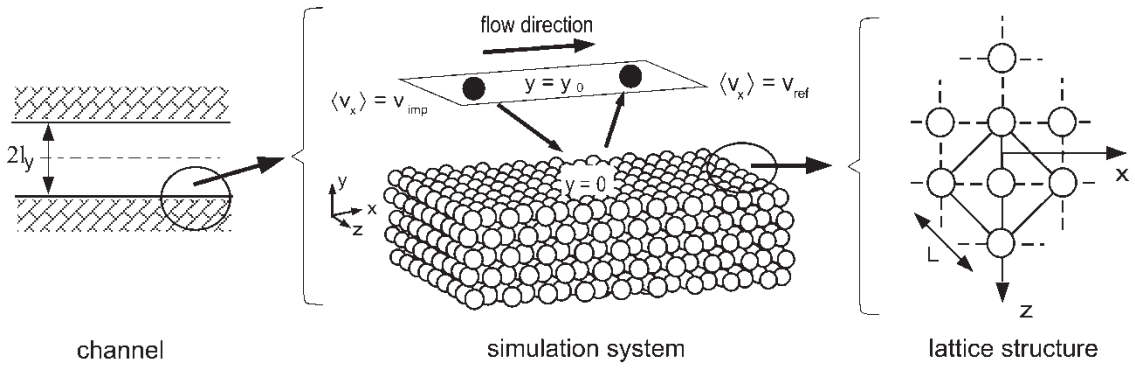


FIGURE 1 Schematic of the molecular dynamics scattering experiment. The circular atoms shown on the rightmost figure belong to the topmost layer of the lattice wall.

be simulated to obtain adequate statistics depends of the magnitude of $v_{imp}$; large impinging velocities require fewer collision events to adequately sample $f$.

The wall surface is modeled as a cleaved [101] face of an fcc lattice with a unit cell length $L$. The lattice is composed of LJ atoms with interaction parameters given by $\sigma_w$ and $\epsilon_w$. The bombarding gas molecules are also represented by the LJ potential with interaction parameters given by $\sigma_g$ and $\epsilon_g$. The interaction between the gas and wall atoms is therefore, represented by the mixed-interaction parameters $\sigma_{wg}$ and $\epsilon_{wg}$ obtained using the standard Lorentz–Berthelot combining rule. The lattice wall is periodic in the lateral directions, i.e. $x$ and $z$ directions, hence periodic boundary conditions are used in these directions to mimic a boundless wall. To reduce the computational effort, the interaction potential between gas molecules and lattice is stored over a three dimensional grid, and an interpolation scheme is used to rapidly compute the potential and forces on the gas molecules during the simulation at any position [29]. A potential cutoff of $3\sigma_{wg}$ is used consistently throughout the simulations. The equations of motion of the colliding molecules are integrated using the velocity Verlet algorithm with a timestep of 2 fs [30].

For this initial study, the simplest possible system is considered, namely a rigid lattice, a spherical gas molecule and a LJ potential. A flexible lattice was also simulated for the case of light gas molecules (16 amu molecular weight). No differences were observed between the results with the flexible lattice and a rigid one, but heavier gas molecules may possibly show differences. Incorporation of a flexible lattice as well as other realistic features into the model such as multi-atom molecular gas species and more realistic surface potential may yield slightly different values for the accommodation coefficient [24,27], and will be the subject of future work. However, it is anticipated that that the current model captures most of the essential physics responsible for slip in these systems.

### Input Velocity Distribution

Consider the gas molecules impinging on the wall which are crossing the plane $y = y_0$ at the beginning of the scattering experiment (see Fig. 1). The velocity of these molecules in the directions parallel to the wall surface (as represented by $v_{\parallel}$) is assumed to be given by the Maxwell–Boltzmann distribution

$$\frac{dN_{v_\parallel}}{N} = \left(\frac{m}{2\pi k_B T}\right)^{1/2} \exp\left(-\frac{m v_\parallel^2}{2k_B T}\right) dv_\parallel \qquad (18)$$

where $v_{\parallel}$ ranges from $-\infty$ to $\infty$. This distribution is not applicable for the velocity component perpendicular to the wall, $v_{\perp}$, because molecules with a large $v_{\perp}$ cross the plane $y = y_0$ more frequently than the molecules possessing a small $v_{\perp}$. The velocity distribution for $v_{\perp}$ must therefore, be the Maxwell–Boltzmann distribution multiplied by the frequency with which molecules cross the plane. The frequency with which molecules cross the plane is clearly proportional to $v_{\perp}$. The *normalized* velocity distribution in the direction perpendicular to the wall is therefore given by

$$\frac{dN_{v_\perp}}{N} = v_\perp \left(\frac{m}{k_B T}\right) \exp\left(-\frac{m v_\perp^2}{2k_B T}\right) dv_\perp \qquad (19)$$

Note that the perpendicular velocities range from 0 to $-\infty$ to represent only the molecules traveling towards the wall, and not away from the wall.

To verify the validity of the above velocity distributions, equilibrium molecular dynamics (EMD) simulations were conducted for non-interacting gas molecules confined within a slit-shaped pore. The pore walls were identical to the walls used in the scattering experiments. Periodic boundary conditions were implemented in the directions parallel to the wall. The gas molecules were inserted randomly into the pore and equilibrated with a Metropolis Monte Carlo procedure for a sufficiently long time such that the correct equilibrium density profile along the width of the pore was obtained. The molecules were then given velocities consistent with the Maxwell–Boltzmann distribution at the desired temperature in all three directions. Next, regular microcanonical MD simulations were conducted for a long enough period such that the gas molecules collided with the walls an average of twenty times. The velocity distributions in directions parallel and perpendicular to the wall were computed over the entire pore width as well as at a plane $3\sigma_{wg}$ distance away from the wall. It was observed that the perpendicular and parallel components of the velocity distribution remained very close to the initial Maxwell–Boltzmann distribution when averaged over the entire pore width. At the plane $3\sigma_{wg}$ above the surface, however, the distributions in the parallel and perpendicular directions matched very closely the distributions represented by Eqs. (18) and (19), thus validating the use of these distributions for the scattering simulations. In addition, the velocity distributions of the reflected molecules always matched those of the impinging molecules at $v_{imp} = 0$ which further corroborates that the right input velocity distribution is used.

## RESULTS AND DISCUSSION

### Governing Parameters

The accommodation coefficient $f$ for the model system may depend on a number of factors,

including the nature of the wall-fluid interactions, the flow conditions near the wall, the temperature $T$, and the mass of the gas molecules $m$. Each of these factors was varied to examine its effect on the accommodation coefficient as well as to determine the minimum number of parameters required to specify $f$.

The wall-fluid interactions are related to the potential energy surface (PES) near the wall, $U(x,y,z)$, which in turn is determined by the LJ interaction parameters $\sigma_{wg}$, $\epsilon_{wg}$ and the lattice geometry. The lattice geometry depends on the six unit cell parameters $(a,b,c,\alpha,\beta,\gamma)$. For an fcc lattice, the only adjustable parameter that remains is the cubic unit cell length $L(=a=b=c)$. Thus the PES is a function of three variables

$$U(x,y,z) = U(\sigma_{wg}, \epsilon_{wg}, L) \tag{20}$$

The flow near the surface is described by the impinging velocity, $v_{imp}$, as introduced in the last section. If the mass of the gas molecule and system temperature are also regarded as variables on which $f$ may depend, then it is expected that

$$f = f(\sigma_{wg}, \epsilon_{wg}, T, v_{imp}, m, L) \tag{21}$$

The number of parameters $f$ depends upon may be reduced by considering a corresponding states non-dimensionalization of these parameters, as outlined below.

For a PES where the fluid-wall atoms interact via the LJ potential, the LJ length parameter may be reduced by the unit cell length and the LJ energy parameter by the thermal energy, such that $\sigma' = \sigma_{wg}/L$ and $\epsilon' = \epsilon_{wg}/k_B T$. If this non-dimensionalization is valid, Eq. (21) may be written as

$$f = f(\sigma', \epsilon', v_{imp}, m) \tag{22}$$

To verify this non-dimensionalization, scattering simulations were first conducted at different values of $\sigma_{wg}$ and $L$, keeping the rest of the parameters in Eq. (22) constant. The mass of the gas molecules was chosen to be 16 amu (to model spherical methane), the temperature was set to 300 K, while $\epsilon_{wg}/k_B$ was set at 100 K. This corresponds to a reduced energy of $\epsilon' = 0.3$. To produce accurate values of $f$, a relatively small impinging velocity was chosen ($v_{imp} = 10$ m/s). As shown below, $f$ is independent of impinging velocity when $v_{imp}$ is of this magnitude. Up to 1 million collisions were simulated for each value of $\sigma'$. Figure 2 shows the result of these calculations for a range of different values of $\sigma'$ at $L = 4, 5,$ and 6 Å. It is clear that $f$ is the same at a given value of $\sigma'$, thus validating this non-dimensionalization.

The parameter $\sigma'$ may be denoted as a "roughness parameter" since it symbolizes the physical roughness of the atomic wall, or more appropriately, of the PES. A small $\sigma'$ signifies a rough wall while a large $\sigma'$ signifies a smooth wall. The results show that gas molecules flowing over a rough wall lose more of their tangential momentum than those flowing over smoother surfaces, implying that the accommodation coefficient decreases as the pores become smoother or as $\sigma'$ increases. The above effect of roughness on $f$ or the slip coefficient has been observed by a few researchers in the past [5,8,24].

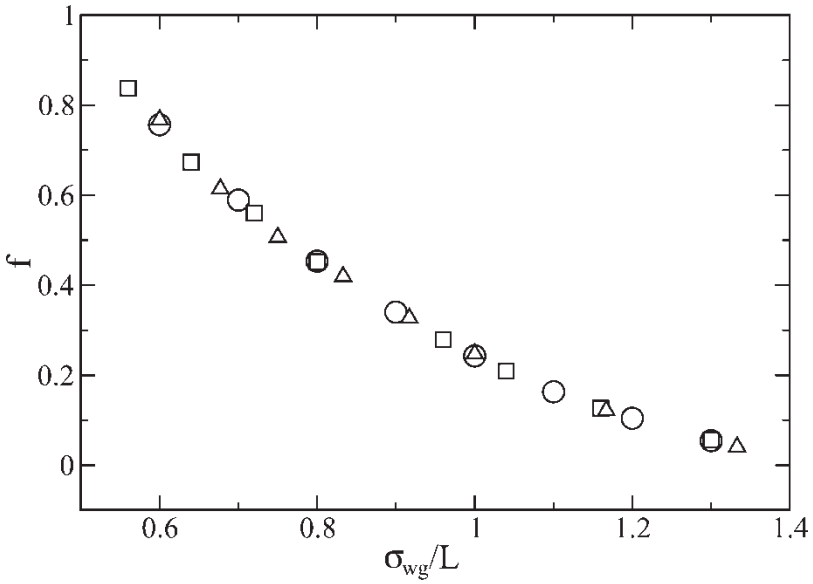


FIGURE 2 Accommodation coefficient $f$ vs. $\sigma_{wg}/L$ for different values of the lattice parameter $L$ at $\epsilon_{wg}/k_B = 100$ K and $T = 300$ K. Open circles, squares and triangles represent lattices having the parameter $L$ equal to 4.0, 5.0 and 6.0 Å, respectively. Error bars smaller than the symbols have not been shown.

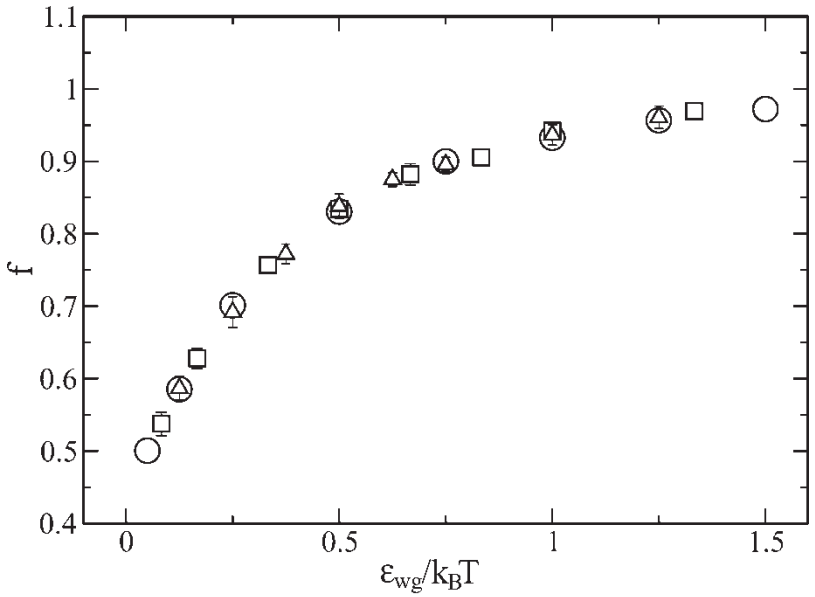


FIGURE 3 Accommodation coefficient vs. $\epsilon_{wg}/k_BT$ for different temperatures at $\sigma_{wg} = 2.4$ Å and $L = 4$ Å. Open circles, squares and triangles represent temperatures of 200, 300 and 400 K, respectively. Error bars smaller than the symbols have not been shown.

Note that the surface simulated here is defect-free, so other factors contributing to the roughness of a real surface, such as displacement/absence of lattice atoms, adsorption of impurities, or mechanical roughening have not been accounted for but are likely to have similar effects on $f$.

To test whether $f$ can be correlated with a reduced energy parameter $\epsilon' = \epsilon_{wg}/k_BT$, a series of scattering simulations were conducted at different temperatures and $\epsilon_{wg}$. Figure 3 shows the computed accommodation coefficients as a function $\epsilon'$ of at temperatures of 200, 300 and 400 K. For these calculations, $\sigma_{wg} = 2.4$ and $L = 4.0$ Å. The mass of the gas molecules, drift velocity and number of sample collisions were chosen to be the same as those used earlier. As expected, the results confirm the validity of using a reduced energy parameter. The accommodation coefficient is observed to rise as the wall-fluid attraction strength increases. By analyzing individual trajectories, it was observed that collisions at low values of $\epsilon'$ were mostly single events, i.e. molecules collided with the wall and immediately bounced back into the gas phase. This behavior gives rise to a large specular component in the collisions, and thus the computed $f$ is close to 0. On the other hand, at large values of $\epsilon'$, gas molecules exhibited multiple collision events with the wall before returning to the bulk gas phase. At $\epsilon' = 1.5$, as many as 50 such collisions were observed as a molecule hopped from one potential minimum to another before finally returning to the bulk phase. As a result of these multiple collisions, the molecules on an average lose their entire drift velocity or the momentum associated with it before they return to the bulk phase, thus resulting in $f$ values being close to unity. Since the gas molecules have a tendency to get adsorbed onto the wall surface at moderate to large values of $\epsilon'$, the process of tangential momentum loss is activated i.e. the accommodation coefficients tends to behave in an Arrhenius fashion with respect to the temperature $T$, as can be observed in Fig. 3.

A similar analysis, in which scattering simulations were conducted with the mass of the gas molecule varying from 1 to 128 amu while holding all else constant, showed that the accommodation coefficient is independent of mass for a rigid lattice. This is to be expected for a rigid wall model, but the mass of a gas molecule may play a role in determining $f$ for a real, flexible surface capable of exchanging momentum with the incoming gas molecule.

Finally, the role the impinging "drift velocity" had on $f$ was also examined. It is expected that $f$ strongly depends on the angle at which the gas molecules collide with the wall surface as well as the velocity they possess. At zero drift velocity, the *mean* angle at which the molecules collide with respect to the surface normal is zero. At finite drift velocities, the mean angle is non-zero and increases monotonically with the magnitude of the drift velocity. To investigate the exact nature of the dependence of $f$ on the drift velocity $v_{imp}$, a series of simulations were conducted at drift velocities ranging from 1 to 1000 m/s, keeping the rest of the governing parameters fixed. Since the statistical accuracy of $f$ decreases with decreasing magnitude of $v_{imp}$, the simulations at small drift velocities required many more collisions than those at high drift velocity. The collision samples therefore, ranged from 10,000 to 10 million corresponding to the largest and

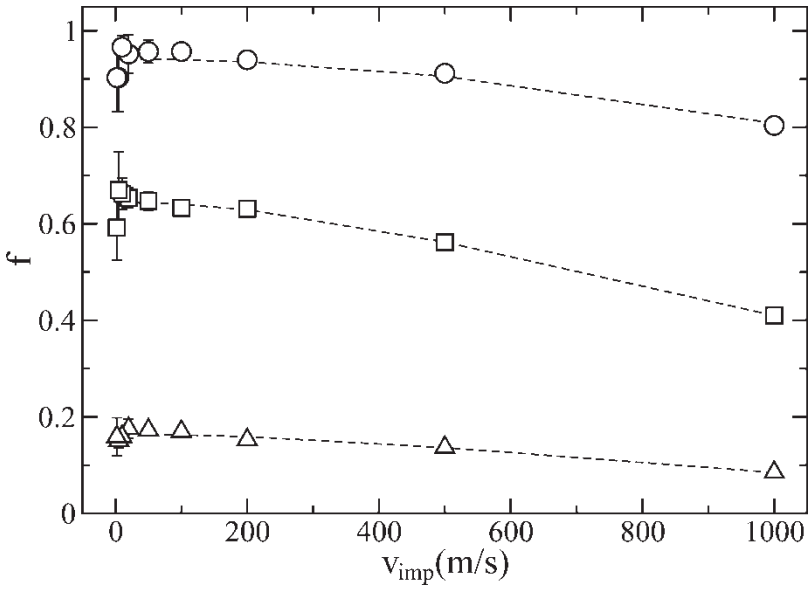


FIGURE 4 Accommodation coefficient as a function of the drift velocity. Open circles correspond to $\sigma_{wg}/L = 0.6$ and $\epsilon_{wg}/k_BT = 1.2$; open squares correspond to $\sigma_{12}/L = 0.8$ and $\epsilon_{wg}/k_BT = 0.7$; while open diamonds correspond to $\sigma_{wg}/L = 1.0$ and $\epsilon_{wg}/k_BT = 0.2$. The dashed lines represent a fit to the data so as to guide the eye.

smallest drift velocities employed, respectively. Figure 4 shows a plot of $f$ vs. $v_{imp}$ at three different values of $\sigma'$ and $\epsilon'$. The accommodation coefficient remains constant at low drift velocities, i.e. $v_{imp} < 100\,m/s$, which is on the order of the thermal velocities of the gas molecules in a given direction. For drift velocities greater than this value, the accommodation coefficient decreases monotonically with increasing drift velocity. This trend may be explained by the fact that at high drift velocities, a large fraction of the collisions occur at glancing angles with the wall surface. At such large collision angles, the potential minima on the surface of the wall are not easily accessible to these molecules. Hence, the impinging molecules simply reflect after colliding with the wall atoms, losing only a little momentum in the process and thus giving rise to smaller accommodation coefficients. At small drift velocities, such effects are negligible and $f$ becomes independent of drift velocity, asymptotically approaching the $v_{imp} = 0$ value. The dependence of $f$ on $v_{imp}$ closely resembles the dependence of shear viscosity on the shear rate in the case of polymers and hydrocarbons i.e. the shear thinning behavior. It should also be noted that, while drift velocities of 100 m/s are much higher than what is to be expected for normal flows, it appears that $f$ reaches an asymptotic value at this velocity. Thus, one can simulate a range of drift velocities and extrapolate to $v_{imp} = 0$ to obtain an estimate of the "true" accommodation coefficient. Importantly, the velocity *distribution* of the reflected molecules (i.e. minus the drift velocity component) remains nearly unchanged from the incident distribution at small drift velocities thus validating that the chosen input velocity distribution represents the correct steady state distribution. At very large drift velocities, the reflected molecules do not maintain this steady state velocity distribution, and hence the computed $f$ is incorrect.

The above analysis suggests that, for small values of $v_{imp}$, $f$ depends only on reduced parameters $\sigma'$ and $\epsilon'$ i.e.

$$f = f(\sigma', \epsilon') \tag{23}$$

Therefore, for a *rigid* lattice, the accommodation coefficient of gases at large Knudsen numbers is simply a function of the morphology of the surface, i.e. its physical roughness and the fluid-wall attraction strength.

### Accommodation Coefficient Vs. $\sigma'$ And $\epsilon'$

The dependence of $f$ on $\sigma'$ and $\epsilon'$ was determined by carrying out a series of simulations with ten different values of the parameter $\sigma'$ ranging from 0.6 to 1.5, and ten different values of the parameter $\epsilon'$ ranging from 0.05 to 1.5 as listed in Table I. Note that in order to avoid gas molecules penetrating the lattice, it was necessary to ensure that $\sigma' > 0.5$. Figure 5 shows the results of these calculations; numerical values are given in Table I. The accommodation coefficient increases with both the roughness and the attractiveness of the wall. Therefore, by tuning the interaction parameters $\sigma'$ and $\epsilon'$ the entire range of $f$ may be explored, i.e. from 0 to 1. Figure 5 thus provides a "phase diagram" that can be used to predict $f$ for any system that can be adequately modeled by the simplified forcefield used in this

TABLE I The computed accommodation coefficient for different wall roughnesses and wall-fluid attractions

| | $\epsilon_{wg}/k_BT$ | | | | | | | | | |
|---|---|---|---|---|---|---|---|---|---|---|
| $\sigma_{wg}/L$ | *0.05* | *0.1* | *0.2* | *0.3* | *0.4* | *0.5* | *0.7* | *1.0* | *1.2* | *1.5* |
| 0.6 | 0.505(5) | 0.559(8) | 0.671(9) | 0.743(7) | 0.802(11) | 0.843(8) | 0.901(6) | 0.933(12) | 0.956(9) | 0.977(11) |
| 0.7 | 0.338(7) | 0.379(9) | 0.471(5) | 0.563(6) | 0.626(3) | 0.689(7) | 0.770(15) | 0.840(9) | 0.875(13) | 0.905(14) |
| 0.8 | 0.219(3) | 0.255(14) | 0.342(8) | 0.422(11) | 0.490(13) | 0.557(2) | 0.654(11) | 0.748(8) | 0.797(11) | 0.854(16) |
| 0.9 | 0.139(5) | 0.169(10) | 0.247(16) | 0.316(14) | 0.376(10) | 0.431(8) | 0.533(8) | 0.653(3) | 0.696(12) | 0.753(10) |
| 1.0 | 0.084(3) | 0.110(2) | 0.170(10) | 0.229(10) | 0.284(10) | 0.328(13) | 0.414(10) | 0.519(7) | 0.578(15) | 0.649(6) |
| 1.1 | 0.044(6) | 0.064(7) | 0.108(4) | 0.154(5) | 0.193(7) | 0.232(10) | 0.295(12) | 0.378(7) | 0.430(10) | 0.505(8) |
| 1.2 | 0.025(1) | 0.038(7) | 0.070(7) | 0.101(2) | 0.131(7) | 0.156(7) | 0.205(7) | 0.270(1) | 0.313(8) | 0.362(4) |
| 1.3 | 0.012(1) | 0.018(1) | 0.037(7) | 0.054(4) | 0.072(4) | 0.085(4) | 0.117(8) | 0.155(5) | 0.182(4) | 0.219(5) |
| 1.4 | 0.006(1) | 0.012(1) | 0.020(5) | 0.029(6) | 0.039(4) | 0.051(2) | 0.068(2) | 0.088(4) | 0.099(3) | 0.117(3) |
| 1.5 | 0.002(1) | 0.005(1) | 0.008(2) | 0.013(4) | 0.017(4) | 0.021(2) | 0.031(3) | 0.039(4) | 0.041(4) | 0.049(4) |

The numbers within parenthesis refer to the uncertainty in the last digit of the computed value of $f$, e.g. $f = 0.316(15)$ implies $f = 0.316 \pm 0.015$

work. An example of such a system is xenon gas flowing through a carbon molecular sieve (CMS). We assume that the fluid–solid interactions for this system can be modeled using the following LJ parameters [31]: $\sigma_{Xe-C} = 3.332\,\text{Å}$ and $\epsilon_{Xe-C} = 132.21\,\text{K}$. The lattice parameter $L$ is taken as half the diagonal of the hexagonal lattice composed of C atoms, which is approximately equal to 5.0 Å. The wall roughness and the attractiveness for the Xe atoms may now be computed as given by

$$\sigma' = \sigma_{Xe-C}/L = 0.67$$
$$\epsilon' = \epsilon_{Xe-C}/k_BT = 0.53 \tag{24}$$

Referring to Fig. 5, the value of the accommodation coefficient for this system is predicted to be equal to 0.75, which suggests that xenon will not exhibit a moderate slip inside CMSs. Unfortunately, no experimental data exists regarding the slip behavior for this system. However, comparison of recent simulation results against experimental molecular beam studies [12] for $N_2$ on z-dol-coated Pt(111) surface shows that quantitative agreement is possible [32].

### Application: Kinetic Separation of Gases

It can clearly be seen from the above results that the accommodation coefficient $f$ is a strong function of the nature of the wall surface, i.e. its atomic roughness and energetic interaction with the gas molecules. This implies that the nature of the wall surface determines the amount of slip at the surface $\zeta$, and consequently the flow rate of gases flowing over such surfaces. As shown earlier, a simple analysis based on Maxwell's theory suggests that two gases which are *identical* to each other in all aspects except in the way they interact with the pore walls may be separated by choosing appropriate

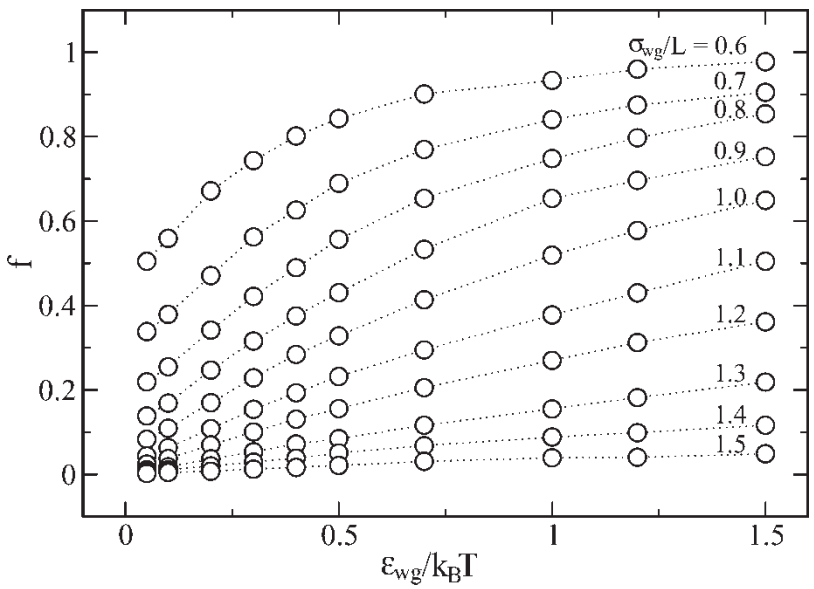


FIGURE 5 Phase diagram showing the dependence of the accommodation coefficient on the parameter $\epsilon_{wg}/k_BT$ at various values of the parameter $\sigma_{wg}/L$. All the error bars are smaller than the symbols and, therefore, are not shown. The dashed lines are meant to guide the eye.

pore wall surfaces which yield different accommodation coefficients for the two gases. Of course, *dissimilar* gases with different accommodation coefficients may also be separated with this technique.

To test Maxwell's model as well as to assess how important $f$ is on the kinetic separation of similar molecules, nonequilibrium molecular dynamics simulations were carried out on a mixture of two gases in a slit pore. Planar Poisueille flow was generated by imposing an external field $\mathbf{F}_e$ on the fluid molecules in a direction parallel to the pore walls [21,33]. The external field mimics the effect of a pressure gradient, $\nabla P$, resulting in a steady flow along the pore. Steady state density profiles, velocities and fluxes are computed, and separation factors determined from Eq. (9).

The upper and lower pore surfaces were modeled using the same fcc atomic wall as that used in the previous scattering simulations. The parameters associated with the fluid–fluid and fluid-wall interactions are summarized below

$$\begin{aligned} &\sigma_{wA}/L = 0.6 \\ &\epsilon_{wA}/k_B T = 1.5 \\ &\sigma_{wB}/L = 1.0 \\ &\epsilon_{wB}/k_B T = 0.5 \\ &\sigma_{AA}/L = \sigma_{BB}/L = \sigma_{AB}/L = 0.8 \\ &\epsilon_{AA}/k_B T = \epsilon_{BB}/k_B T = \epsilon_{AB}/k_B T = 0.4 \end{aligned} \tag{25}$$

where $L$ was set to 4.0 Å, $T$ was set to 300 K, and the molecular mass of both gases was set to 16 amu. The two gases interact similarly amongst themselves and with each other, but differ in the way in which they interact with the wall. Referring to Table I, the accommodation coefficients $f$ for gases A and B are equal to 0.328 and 0.977, respectively. Four pore widths were chosen in the range from 20 to 100 Å, while the gas densities within the pore were varied from an atmospheric gas-like density of 75 mol/m$^3$ to a liquid-like density of 40,000 mol/m$^3$. The simulations were conducted at a constant temperature with a timestep of 2 fs by using a Nosé-Hoover thermostat [30] with a time constant $\tau = 0.5$ ps. The initial configuration was generated by inserting equal number of molecules of both the gas components. The system was then equilibrated using regular molecular dynamics for 1 ns before collecting the data. The pore width was divided into 100 equal-sized bins in order to compute the various profiles of interest for each gas component.

The above nonequilibrium method is mainly applicable for simulating liquid and dense gas flows, but fails to realistically mimic gas flows at large Knudsen numbers. At large $Kn$, the gas molecules accelerate for long periods of time before they collide with the wall or with other gas molecules, thereby gaining unrealistically high velocities in between collisions. The velocity profiles are likely to be inaccurate at large $Kn$, but the separation factors may be more accurate, since they represent the ratio of two quantities having the same degree of uncertainty.

Figure 6 shows the computed separation factors $S_{AB}$ plotted against the Knudsen number for four different pore widths used in the study. Several interesting trends may be observed in the figure.

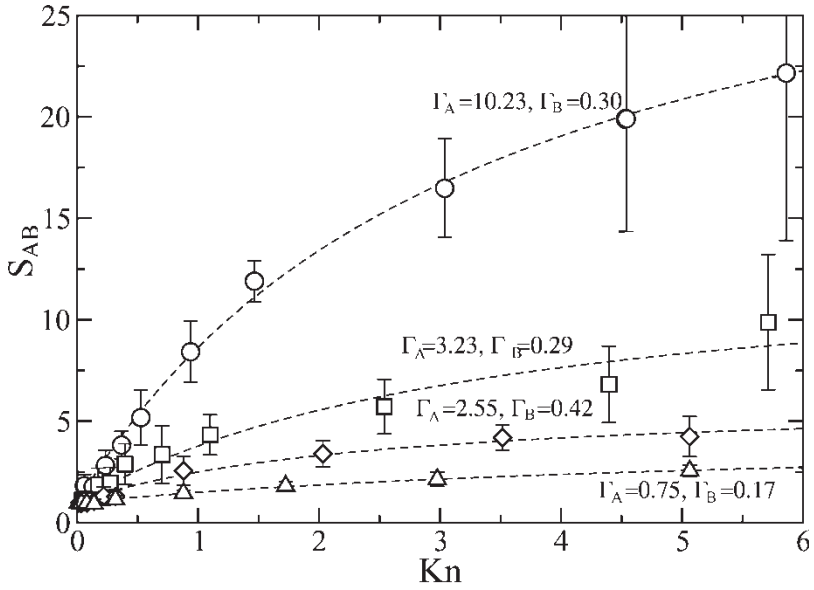


FIGURE 6 Separation factors vs. the Knudsen number for different porewidths. Open circles, squares, diamonds and triangles represent pore widths of 20, 30, 50 and 100 Å, respectively. The dashed lines represent the fits given by the model while the coefficients $\Gamma_A$ and $\Gamma_B$ are the parameters corresponding to each fit.

First, the separation factors tend to increase monotonically with the Knudsen number. It is clear that at low densities, the effect of the wall becomes more important as fluid-wall molecular collisions start to dominate over the fluid–fluid collisions. This results in an increasing slip coefficient for both the gases as the gas becomes more rarefied, thereby causing a rise in the corresponding fluxes, $J_A$ and $J_B$. The separation factor, which is the ratio of the two fluxes, tends to increase as well. The figure clearly shows the separation factor being close to unity at liquid-like densities and then rising as the densities become smaller or $Kn$ becomes larger. Secondly, the separation factors are observed to increase as the pore becomes narrower. As before, the fluid-wall molecular collisions dominate over fluid–fluid collisions as the pores get narrower. Upon close examination of Eq. (2), we observe that the *relative* importance of the slip coefficient, as described by the factor $\zeta/a$, increases as the pore width, $a$, becomes smaller. This implies that the ratio of fluxes $J_A/J_B$ would also increase as the pore width decreases.

The above trends of the separation factor with respect to the fluid density and the pore width are well captured by the model described in "Background" section. Note that both a decrease in the density ($n$) as well as the pore width ($l_y$) causes $Kn$ to increase (refer to Eq. (14)), thereby resulting in an increase in the separation factor $S_{AB}$ in Eq. (15). In essence, the effects of both the fluid density and pore width have been suitably combined in the single parameter $Kn$. The solid lines in Fig. 6 show the result of the model given by Eq. (15) in matching the separation factor obtained from the simulations. Both $\Gamma_A$ and $\Gamma_B$ were adjusted to obtain the best fit to the simulation results in a least-squares fashion. Allowing $\Gamma_A$ and $\Gamma_B$ to be adjusted yields excellent fits to the simulation data, thereby confirming that Eq. (15) shows the correct dependence of $S_{AB}$ on $Kn$. Strictly speaking, $\Gamma_A$ and $\Gamma_B$ are not adjustable parameters and may be computed using Eq. (16). To test the model more rigorously, it is useful to examine its asymptotic limits. The two limits of Eq. (15), i.e. in the limit of large and small $Kn$ are stated below

$$S_{AB} = \begin{cases} \frac{\Gamma_A}{\Gamma_B} = \frac{f_B}{f_A}\left(\frac{2-f_A}{2-f_B}\right) & \text{if } Kn \to \infty \\ 1 & \text{if } Kn \to 0 \end{cases} \tag{26}$$

The above equation clearly suggests that the degree of separation becomes negligible as the pore width and/or density becomes large, such that $Kn \to 0$. It also suggest that the maximum separation is achieved by ensuring that the pore widths are as small as possible, and that the gases are in the Knudsen regime. Applying Eq. (26) to the simulation system shows that the highest possible separation factor is expected to be about 4.9. This is significantly lower than the largest computed value of the separation factor, which is equal to 22.1 for the case of a pore with a width of 20 Å containing fluid at a density of 400 mol/m$^3$. This suggests that the $\Gamma_A$ and $\Gamma_B$ values obtained from the Maxwell's model are different from the values obtained from the fits to the simulation data.

In order to understand the source of these difference, we have plotted the density, velocity and flux profiles of gases A and B along the width of the pore for the above specific pore width and fluid density, as shown in Fig. 7. Notice that the velocity profile for gas A shows a large degree of slip at the pore walls as compared to that of gas B which shows negligible slip. This is clearly due to the difference in the accommodation coefficients of the two gases. The velocity of gas A is, therefore, larger than that of gas

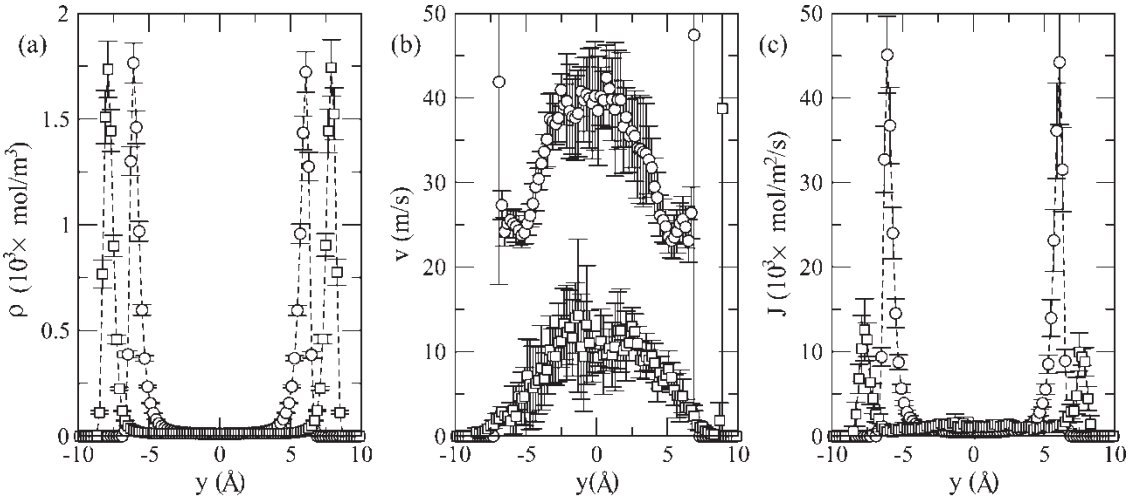


FIGURE 7 Transverse (a) density, (b) velocity and (c) flux profiles for a 20 Å wide pore at an average density of 400 mol/m$^3$. The circles represent gas *A* while the squares represent gas *B*. The fluxes for gas *B* in (c) have been multiplied by a factor of 10 so as to make then clearly visible.

B at all positions along the pore width, which gives rise to a higher flux. The density profiles of the two gases show that significant adsorption occurs close to the wall surfaces due to their attractive nature. It can observed that these adsorbed molecules in the case of gas A flow at finite velocities, while those corresponding to gas B remain close to stationary. Due to the above reason, the separation factor close to the wall surfaces is very large. Additionally, since a majority of the gas molecules tend to reside close to the wall surface, most of the separation occurs near the wall surface. The major source of the error in the theory is therefore, the assumption that the density profile of the gas is uniform across the pore width. The simulation results clearly indicate that there is a significant enhancement of the density near the wall surface. Because most gas molecules are near the wall, small differences in the slip length near the wall surface can give rise to dramatic differences in total flux, as seen in the simulations. The simplified model with the assumption of a uniform density profile thus provides a lower bound for $S_{AB}$. Future work will be directed toward improving the model by accounting for variation in density along the pore width.

An interesting result emerges when we compute the self-diffusivities and the phenomenological coefficients of the two components as represented by $D_{AA}$ and $D_{BB}$ and $L_{AA}$ and $L_{BB}$, respectively, for the above particular porewidth and fluid density. This was done by applying both the Green-Kubo and Einstein formulations using equilibrium molecular dynamics simulations [34]. It was found that the ratios $D_{AA}/D_{BB}$ and $L_{AA}/L_{BB}$ closely matched the separation factor obtained from the nonequilibrium simulations. Since most of the gas molecules reside close to the wall, the above ratios indicate the relative mobility of one species over the other in the adsorbed state close to the wall. These results suggest that the accommodation coefficient or the degree of slip at the surface is closely related to the mobility of molecules adsorbed near the wall.

## CONCLUSIONS

A simple and efficient molecular dynamics technique has been developed for computing the tangential momentum accommodation coefficient of dilute gases flowing over surfaces. The accommodation coefficient is an important factor governing the amount of slip occurring at the surface. The technique involves determining the average loss in the tangential momentum of gas molecules bombarding a rigid wall surface. It was shown that the accommodation coefficient is primarily dependent on the morphology of the wall surface, i.e. its atomic roughness and its energetic attraction to the gas molecules. Both these factors have been quantified in the form of dimensionless parameters involving the LJ interaction parameters. The dependence of the accommodation coefficient on the two factors has been conveniently presented in two-dimensional plots such that the accommodation coefficient may easily be obtained for an experimental surface-gas system where the governing parameters are known *a priori*. It has also been shown that molecular inertia does not plays any role on the magnitude of the accommodation coefficient for a rigid wall surface, and that the accommodation coefficient remains constant at flow velocities on the order of those found in real micropores, but decreases at very high flow velocities.

It was also demonstrated how small differences in slip coefficients can be exploited for the kinetic separation of gases. Two *identical* gases differing only in the way they interact with the pore wall can be separated based on differences in their accommodation coefficients. Pore widths as small as 20 Å have been shown to yield separation factors as large as 22 at gas densities similar to the atmospheric density. An analytic model based on Maxwell's theory provides a lower bound to the achievable separation factor.

### *Acknowledgements*

Computational resources were provided by a grant from the National Science Foundation (DMR 79647). Acknowledgment is made to the Donors of The Petroleum Research Fund, administered by the American Chemical Society, for partial support of this research. GA acknowledges the Center for Applied Mathematics at Notre Dame for a fellowship. HCC acknowledges support from the Bayer chair fund and an NSF-XYZ-on-a-chip grant (CTS99-80745).

### *References*

[1] Karniadakis, G.E. and Beskok, A. (2002) *Micro Flows-Fundamentals and Simulation* (Springer, New York).
[2] Gad-el-Hak, M. (2001) *The CRC Handbook of MEMS* (CRC Press, Boca Raton).
[3] Khare, R., de Pablo, J.J. and Yethiraj, A. (1996) "Rheology of confined polymer melts", *Macromolecules*, **29**, 7910.
[4] Barsky, S. and Robbins, M.O. (2001) "Molecular dynamics study of slip at the interface between immiscible polymers", *Phys. Rev. E* **63**, 021801.
[5] Pit, R., Hervet, H. and Léger, L. (2000) "Direct experimental evidence of slip in hexadecane: solid interfaces", *Phys. Rev. Lett.* **85**, 980.
[6] Zhu, Y. and Granick, S. (2002) "Limits of the hydrodynamic no-slip boundary condition", *Phys. Rev. Lett.* **88**, 106102.
[7] Zhu, Y. and Granick, S. (2001) "Rate-dependent slip of Newtonian liquid at smooth surfaces", *Phys. Rev. Lett.* **87**, 096105.
[8] Thompson, P.A. and Troian, S.M. (1997) "A general boundary condition for liquid flow at solid surfaces", *Nature* **389**, 360.

[9] Tretheway, D.C. and Meinhart, C.D. (2002) "Apparent fluid slip at hydrophobic microchannel walls", *Phys. Fluids* **14**, L9.
[10] Millikan, R.A. (1923) "Coefficients of slip in gases", *Phys. Rev.* **21**, 217.
[11] Kennard, E.H. (1938) *Kinetic Theory of Gases* (McGraw-Hill, New York).
[12] Rettner, C.T. (1998) "Thermal and tangential-momentum accommodation coefficients for $N_2$ colliding with surfaces of relevance to disk-drive air bearings derived from molecular beam scattering", *IEEE T. Magn.* **34**, 2387.
[13] Megaridis, C.M., Yazicioglu, A.G., Libera, J.A. and Gogotsi, Y. (2002) "Attoliter fluid experiments in individual closed-end carbon nanotubes: liquid film and fluid interface dynamics", *Phys. Fluids* **14**, L5.
[14] Travis, K.P. (2002) "Computer simulation investigation of diffusion selectivity in graphite slit pores", *Mol. Phys.* **100**, 2317.
[15] Gabis, D.H., Loyalka, S.K. and Storvick, T.S. (1996) "Measurements of the tangential momentum accommodation coefficient in the transition flow regime with a spinning rotor gauge", *J. Vac. Sci. Technol. A* **14**, 2592.
[16] Tekasakul, P., Bentz, J.A., Thomson, R.V. and Loyalka, S.K. (1996) "The spinning rotor gauge: measurements of viscosity, velocity slip coefficients and tangential momentum accommodation coefficients", *J. Vac. Sci. Technol. A* **14**, 2946.
[17] Bentz, J.A., Thomson, R.V. and Loyalka, S.K. (1997) "The spinning rotor gauge: measurements of viscosity, velocity slip coefficients and tangential momentum accommodation coefficients for $N_2$ and $CH_4$", *Vacuum* **48**, 817.
[18] Bentz, J.A., Thomson, R.V. and Loyalka, S.K. (2001) "Measurements of viscosity, velocity slip coefficients and tangential momentum accommodation coefficients using a modified spinning rotor gauge", *J. Vac. Sci. Technol. A* **19**, 317.
[19] Arkilic, E.B., Breuer, K.B. and Schmidt, M.A. (2001) "Mass flow and tangential momentum accommodation in silicon micromachined channels", *J. Fluid. Mech.* **437**, 29.
[20] Veijola, T., Kuisma, H. and Lahdenperä, J. (1998) "The influence of gas-surface interaction on gas-film damping in a silicon accelerometer", *Sensor Actuator* **66**, 83.
[21] Travis, K.P. and Gubbins, K.E. (2000) "Poiseuille flow of Lennard–Jones fluids in narrow slit pores", *J. Chem. Phys.* **112**, 1984.
[22] Khare, R., de Pablo, J.J. and Yethiraj, A. (1997) "Molecular simulation and continuum mechanics study of simple fluids in non-isothermal planar couette flows", *J. Chem. Phys.* **107**, 2589.
[23] Sokhan, V.P., Nicholson, D. and Quirke, N. (2001) "Fluid flow in nanopores: an examination of hydrodynamic boundary conditions", *J. Chem. Phys.* **115**, 3878.
[24] Sun, M. and Ebner, C. (1992) "Molecular dynamics study of flow at a fluid-wall interface", *Phys. Rev. Lett.* **69**, 3491.
[25] Cieplak, M., Koplik, J. and Banavar, J.R. (2001) "Boundary conditions at a fluid–solid Interface", *Phys. Rev. Lett.* **86**, 803.
[26] Cieplak, M., Koplik, J. and Banavar, J.R. (2000) "Molecular Dynamics of Flows in the Knudsen Regime", *Physica A* **287**, 153.
[27] Jabbarzadeh, A., Atkinson, J.D. and Tanner, R.I. (1999) "Wall slip in the molecular dynamics simulation of thin films of hexadecane", *J. Chem. Phys.* **110**, 2612.
[28] Hess, S. and Loose, W. (1989) "Slip flow and slip boundary coefficient of a dense fluid via nonequilibrium molecular dynamics", *Physica A* **162**, 138.
[29] June, R.L., Bell, A.T. and Theodorou, D.N. (1990) "Molecular-dynamics study of methane and xenon in silicalite", *J. Phys. Chem.* **94**, 8232.
[30] Allen, M.P. and Tildesley, D.J. (1987) *Computer Simulations of Liquids* (Clarendon Press, Oxford).
[31] Simonyan, V.V., Johnson, J.K., Kuznetsova, A. and Yates, J.T. (2001) "Molecular simulation of xenon adsorption on single-walled carbon nanotubes", *J. Chem. Phys.* **114**, 4180.
[32] G. Arya, PhD thesis, Department of Chemical Engineering, University of Notre Dame, Notre Dame, IN (2003).
[33] Todd, B.D., Evans, D.J. and Daivis, P.J. (1995) "Pressure tensor for inhomogeneous fluids", *Phys. Rev. E* **52**, 1627.
[34] Sanborn, M.J. and Snurr, R.Q. (2000) "Diffusion of binary mixtures of $CF_4$ and n-alkanes in faujasite", *Sep. Purif. Technol.* **20**, 1.